Available online at www.sciencedirect.com
ScienceDirect
Journal of Power Sources 165 (2007) 171–184
JOURNAL OF POWER SOURCES
www.elsevier.com/locate/jpowsour

Transient computation fluid dynamics modeling of a single proton exchange membrane fuel cell with serpentine channel

Hu Guilin [a,b], Fan Jianren [b,*]

[a] School of Light Industry, Zhejiang University of Science and Technology, Hangzhou 310023, PR China
[b] State Key Laboratory of Clear Energy Utilization, Zhejiang University, Hangzhou 310027, PR China

Received 8 September 2006; received in revised form 23 November 2006; accepted 23 November 2006
Available online 22 January 2007

Abstract

The proton exchange membrane fuel cell (PEMFC) has become a promising candidate for the power source of electrical vehicles because of its low pollution, low noise and especially fast startup and transient responses at low temperatures. A transient, three-dimensional, non-isothermal and single-phase mathematical model based on computation fluid dynamics has been developed to describe the transient process and the dynamic characteristics of a PEMFC with a serpentine fluid channel. The effects of water phase change and heat transfer, as well as electrochemical kinetics and multicomponent transport on the cell performance are taken into account simultaneously in this comprehensive model. The developed model was employed to simulate a single laboratory-scale PEMFC with an electrode area about 20 cm^2. The dynamic behavior of the characteristic parameters such as reactant concentration, pressure loss, temperature on the membrane surface of cathode side and current density during start-up process were computed and are discussed in detail. Furthermore, transient responses of the fuel cell characteristics during step changes and sinusoidal changes in the stoichiometric flow ratio of the cathode inlet stream, cathode inlet stream humidity and cell voltage are also studied and analyzed and interesting undershoot/overshoot behavior of some variables was found. It was also found that the startup and transient response time of a PEM fuel cell is of the order of a second, which is similar to the simulation results predicted by most models. The result is an important guide for the optimization of PEMFC designs and dynamic operation.

Keywords: Proton exchange membrane fuel cell; Transient model; Computation fluid dynamics

1. Introduction

A proton exchange membrane fuel cell has many useful characteristics, especially a short startup time at normal temperature, which makes it a promising power source for future transportation, such as in electrical vehicles. General speaking, PEMFCs as power sources for transportation will often operate dynamically, for example during startup and stop, acceleration and deceleration of electrical vehicles. Thus, explicit knowledge of the transient behavior of a PEMFC is becoming an important research subject, and is important not only for the design of the controllers but also for the optimization of transient cell performance during changes in some operating cases.

Hitherto, there have lots of numerical investigations on PEMFCs, however, most of them are based on steady and single-phase mathematical models and are focused on a single channel of a simple cell structure such as a straight channel [1–4]. By contrast, dynamic models and corresponding numerical simulations are rare. Some interesting and significant contributions have mainly been done by the researchers and groups including Amphlett et al. [5] and Wöhr et al. [6] who mainly studied the dynamic responses to fuel cell temperature. Van Bussel et al. [7] simulated the polarization characteristics of a cell using a two-dimensional, dynamic model. Based on computation fluid dynamics model, Um and Wang [8] tried simulating the dynamic response of the current density to a step change in cell voltage for the first time. Yerramalla et al. [9] conducted linear and non-linear analysis of a PEMFC system in order to know the whole and complex dynamic characteristics. Pathapati et al. [10] solved the transient response of characteristic parameters to a step change in current density using SIMULINK. Wang and

* Corresponding author. Tel.: +86 571 87951764; fax: +86 571 87951764.
E-mail address: fanjr@zju.edu.cn (J. Fan).

0378-7753/$ – see front matter © 2006 Elsevier B.V. All rights reserved.
doi:10.1016/j.jpowsour.2006.11.084

Nomenclature

A	operation area of cell (m^2)
A_{cv}	specific surface area of the control volume (c.v.) (m^{-1})
C_i	mass fraction of chemical species i ($kg\,kg^{-1}$)
C_p	constant-pressure heat capacity ($J\,kg^{-1}\,K^{-1}$)
D_i^{eff}	effective diffusion coefficient of species i ($m^2\,s^{-1}$)
F	Faraday constant ($96487\,C\,mol^{-1}$)
G	flux
h_{fg}	latent heat of water phase change ($kJ\,kg^{-1}$)
I_{avg}	average current density ($A\,m^{-2}$)
$I_{O_{H_2}}$	anode exchange current density ($A\,m^{-2}$)
$I_{O_{O_2}}$	cathode exchange current density ($A\,m^{-2}$)
$I(x, y)$	local current density ($A\,m^{-2}$)
K	permeability of porous media (m^2)
K_c	condensation rate constant (s^{-1})
K_v	vapourisation rate constant ($(Pa\,s)^{-1}$)
M_i	molecular weight of species i ($kg\,mol^{-1}$)
n	number of electrons in electrochemical reaction
p	pressure of fluid (Pa)
p_{H_2}	hydrogen partial pressure (Pa)
p	oxygen partial pressure (Pa)
r	stoitriometry coefficient in electrochemical reaction
R	universal gas constant ($8.314\,J\,mol^{-1}\,K^{-1}$)
R_{fc}	cell resistance
s	saturation of liquid water
S	source term
ΔS	entropy change for cell reaction ($J\,K^{-1}$)
t	time (s)
T	temperature (K)
$\boldsymbol{u}$	intrinsical fluid velocity vector ($m\,s^{-1}$)
V_{oc}	cell open-circuit voltage (V)
X_k	mole fraction of species k

Greek letters

$\alpha(x, y)$	net water flux per proton flux
ε	porosity of porous media
$\eta(x, y)$	local activation overpotential (V)
λ^{eff}	effective heat conductivity
μ^{eff}	effective dynamic viscosity ($kg\,s\,m^{-2}$)
θ	stoichiometry flow ratio
ρ	density of the mixture ($kg\,m^{-3}$)
σ_{mem}	local ionic conductivity of membrane ($(\Omega\,m)^{-1}$)

Subscripts

a	anode
c	cathode
i	species
k	anode or cathode
m	mass
T	temperature
u	momentum
wl	liquid water
wv	water vapor

Superscripts

eff	effective
sat	saturation

Wang [11] estimated various time constants for important transport phenomena and analyzed characteristic parameter variation with time during step changes in cell voltage and the humidity of the inlet gas stream. Van Zee and co-workers [12,13] have conducted many experimental studies and dynamic simulations of a PEMFC. However, there have not been comprehensive studies of the characteristic parameters during startup and step changes in operation, in particular, transient single-phase modeling on a complex structure cell with a serpentine fluid channel cannot be found in the published literature.

The objective of this study is two-fold. One goal is to develop a transient, three-dimensional, single-phase model based on computational fluid dynamics. The second goal with practical importance is to investigate the transient process of a PEMFC, such as to numerically analyze the transient response to fluid flow, reactant concentration, temperature and current density and so on, in a single fuel cell during startup and step changes and sinusoidal changes in operating cases. A complex cell structure with serpentine flow fields was used as the research object in this paper.

2. Description of the mathematical model

The computational domain for this model is a whole single cell with electrode area 4.1 cm × 5.2 cm and single serpentine fluid channel having 20 flow paths, as illustrated in Fig. 1. The bipolar plate of the fuel cell is shown in Fig. 1(a), in which flow paths for the reactants and products are carved. The other components across the membrane excluding the bipolar plate are shown in Fig. 1(b), including seven components: fluid channels, diffusion layers and catalyst layers of the anode and the cathode, and proton exchange membrane in the middle of the cell.

The following simplifying assumptions have been used in this model development:

(1) The flow in fuel cell is laminar everywhere. This is reasonable for the low velocity and low Reynolds number.
(2) The proton membrane is impermeable to gas species.
(3) Isothermal boundary conditions are used for the external wall and inlet stream.
(4) The porous media such as the diffusion layer and the catalyst layer are isotropic and homogeneous, characterized by effective permeability and uniform porosity.
(5) Transients in water accumulation in the membrane are neglected in this model, but are considered in Wang and Wang [14].

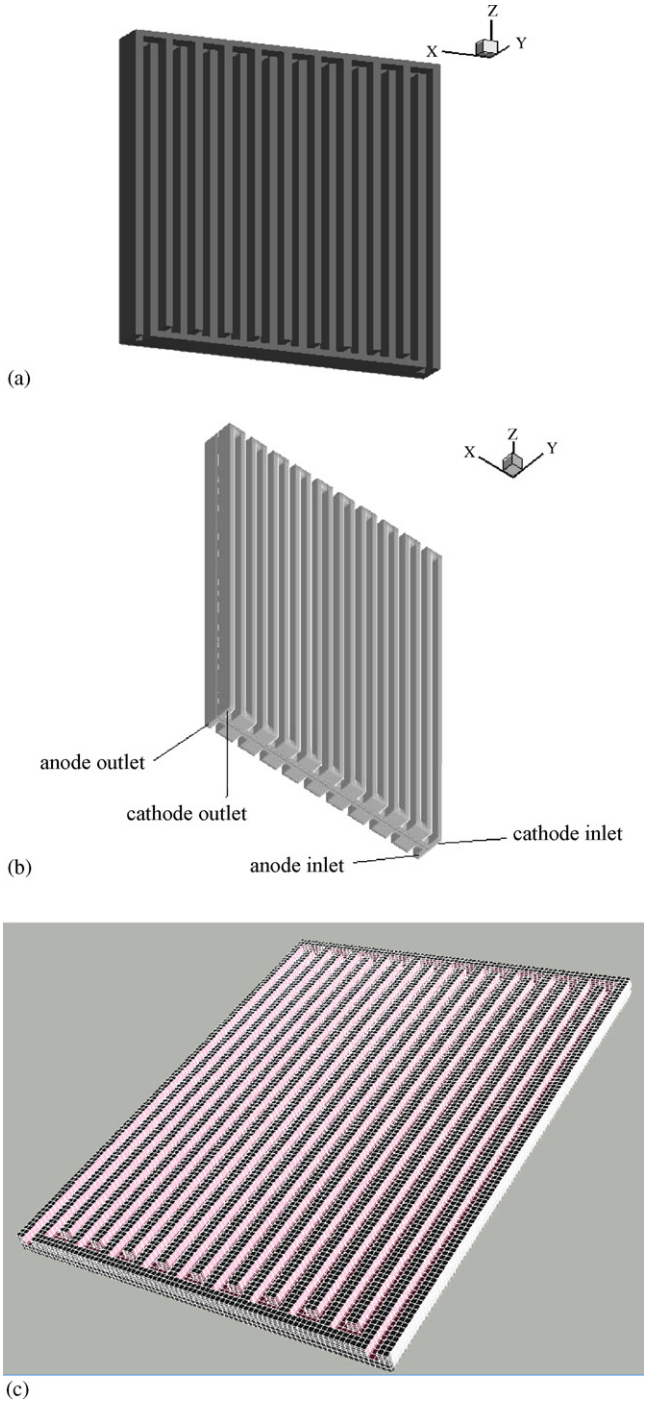

Fig. 1. Schematic of channel structure, components and grid partition of a single fuel cell. (a) Bipolar plate and channel structure, (b) components across membrane and (c) Numerical grid of the bipolar plate.

(6) Water is generated in the catalyst layer in the form of vapor; condensation occurs after vapor partial pressure exceeds saturation vapor pressure. This is the weakest flaw in this non-isothermal model, and will be improved in our future work.

2.1. Governing equation

Numerical simulation is based on a transient, three-dimensional, multicomponent, non-isothermal and single-phase transportation model, which is a comprehensive model including mass, momentum, energy and chemical component transportation. The conservation equations appear as the same form for the fluid channels, the diffusion layers, the catalyst layers and the membrane, but with different coefficients and sources because the catalyst layers and diffusion layers are porous media. Thus, the mathematical model can be described as following:

Continuum equation

$$\frac{\partial(\varepsilon\rho)}{\partial t} + \nabla\cdot(\varepsilon\rho\boldsymbol{u}) = S_m \tag{1}$$

Momentum equation

$$\frac{\partial(\varepsilon\rho\boldsymbol{u})}{\partial t} + \nabla\cdot(\varepsilon\rho\boldsymbol{u}\boldsymbol{u}) = -\varepsilon\nabla p + \nabla\cdot(\varepsilon\mu^{\text{eff}}\nabla\boldsymbol{u}) + S_u \tag{2}$$

Species conservation equation

$$\frac{\partial(\varepsilon\rho C_i)}{\partial t} + \nabla\cdot(\varepsilon\rho\boldsymbol{u}C_i) = \nabla\cdot(-\rho D_i^{\text{eff}}\nabla C_i) + S_i \tag{3}$$

Energy conservation equation

$$\frac{\partial(\rho C_p T)}{\partial t} + \nabla\cdot(\rho\boldsymbol{u}C_p T) = \nabla\cdot(\lambda^{\text{eff}}\nabla T) + S_T \tag{4}$$

The mass source term in continuum equation is described as following [15,16]:

$$S_m = \begin{cases} 0, & \text{others} \\ \sum_i S_i, & \text{catalyst layer} \end{cases} \tag{5}$$

where S_i is source term of species i, such as hydrogen, water vapor, liquid water, oxygen. In the channels and diffusion layers, mass source term is zero because that water vapor decreases equals to liquid water increases for condensation, so the total source is zero. Because chemical reaction can cause consumption and production of species, mass source term can be described as

$$S_i = \frac{r}{nF} I(x,y) M_i A_{\text{cv}} \tag{6}$$

Considering water production in the cathode catalyst layer, mass transfer of water through membrane for the electroosmosic with proton, and phase change between water vapor and liquid water, source term of water vapor can be written as

$$S_{\text{w,c}} = \frac{1+2\alpha(x,y)}{2F} I(x,y) M_{\text{H}_2\text{O}} A_{\text{cv}} + S_{\text{wv}_p} \tag{7}$$

$$S_{\text{w,a}} = -\frac{\alpha(x,y)}{F} I(x,y) M_{\text{H}_2\text{O}} A_{\text{cv}} + S_{\text{wv}_p} \tag{8}$$

where the source term of water vapor induced by phase change can be defined as

$$S_{\text{wv}_p} = k_{\text{c}} \frac{\varepsilon\cdot(1-s) M_{\text{H}_2\text{O}}\cdot C_{\text{H}_2\text{O}}}{RT} [p_{\text{wv}}^{\text{sat}} - p_{\text{wv}}] \,\text{sgn}(p_{\text{wv}} - p_{\text{wv}}^{\text{sat}}) + k_{\text{v}}\varepsilon\rho_l s (p_{\text{wv}} - p_{\text{wv}}^{\text{sat}}) \,\text{sgn}(p_{\text{wv}}^{\text{sat}} - p_{\text{wv}}) \tag{9}$$

Correspondingly, the source term for liquid water can be determined as

$$S_{\mathrm{wl}_p} = -S_{\mathrm{wv}_p} \tag{10}$$

For the momentum equation, the source term read as follows:

$$S_u = \begin{cases} 0, & \text{fluid channel} \\ \dfrac{\mu^{\mathrm{eff}}}{K}\varepsilon\varepsilon\boldsymbol{u}, & \text{diffusion layer/catalyst layer} \end{cases} \tag{11}$$

The non-zero term in above equation indicates the interaction force between fluid and solid base in the porous media.

The source term for energy conservation equation can be written as

$$S_T = \begin{cases} S_{\mathrm{wl}_p} \times h_{\mathrm{fg}}, & \text{fluid channel and diffusion layer} \\ I(x,y) \times A_{\mathrm{cv}} \times \left(\dfrac{-T\Delta S}{nF} + \eta\right) + S_{\mathrm{wl}_p} \times h_{\mathrm{fg}}, & \text{catalyst layer} \\ \dfrac{I(x,y)^2}{\sigma_{\mathrm{mem}}}, & \text{membrane} \end{cases} \tag{12}$$

For the channel and diffusion layer, latent heat of water phase change is considered and ohm heat of current is neglected because the electronic conductivity is very large; for the catalyst layer, the reversible and irreversible reaction heat as well as latent heat of water phase change are considered; for the membrane, ohm heating of current is considered because the resistance of membrane is large.

2.2. Relation between voltage and current density

Taking into account the voltage loss induced by ohm resistance and activation polarization, the actual cell voltage of a fuel cell can be explained as

$$V_{\mathrm{cell}} = V_{\mathrm{oc}} - \eta(x,y) - I(x,y) \cdot R_{\mathrm{fc}} \tag{13}$$

The local activation overpotential $\eta(x, y)$ is composed of two parts: anode activation overpotential and cathode activation overpotential, and the latter occupies main part, can be given by following equation:

$$\eta(x,y) = \frac{RT(x,y)}{0.5F} \ln\left[\frac{I(x,y)\cdot p(x,y)}{I_{\mathrm{O}_2} p_{\mathrm{O}_2}(x,y)}\right] + \frac{RT(x,y)}{1.0F} \ln\left[\frac{I(x,y)\cdot p(x,y)}{I_{\mathrm{O}_{\mathrm{H}_2}} p_{\mathrm{H}_2}(x,y)}\right] \tag{14}$$

The ohm resistance includes electrode and membrane resistance, read as

$$R_{\mathrm{fc}} = \frac{\sigma_{\mathrm{mem}}}{t_{\mathrm{mem}}} + \frac{\sigma_{\mathrm{a}}}{t_{\mathrm{bla}}} + \frac{\sigma_{\mathrm{c}}}{t_{\mathrm{blc}}} \tag{15}$$

2.3. Initial and boundary conditions

For species concentration and temperature, the same values at inlet are applied as the initial conditions. The initial condition of velocity can be obtained by solving flow equation without reaction to reach stable state. Flow rate required for fuel and air electrode is a function of the desired current density and the stoichiometry flow ratio, which can be determined by following equation:

$$G_k = \theta \frac{I_{\mathrm{avg}} A}{2F} \frac{RT}{pX_k} \tag{16}$$

Furthermore, fluid velocity required for the inlet stream can be obtained.

Velocity, species concentration and temperature at the inlet are specified according to the cell operating conditions, viz. first kind boundary condition. At the outlet, pressure outlet boundary (assuming pressure to be zero) is employed; the other variables as temperature, species concentration and fluid velocity are set to be fully developed, that is, the gradient of these variables is equal to zero. For the interface between fluid domain and solid domain, the flux of species is equal to zero, no-slip applies to velocity condition and the coupled boundary condition is set for temperature. The temperature on the external surface of the bipolar plate is specified according to cell operation environment temperature, such as 353.15 K used in this paper.

2.4. Numerical procedure

The whole solution includes three steps corresponding to three main processes of cell operation. First of all, the computation without reaction is conducted until the solution is convergent, which corresponds to the pre-feed reactants and preheating process for fuel cell operation. Secondly, the transient startup process computation using results of previous process as initial value is conducted, and until the new steady-state value is obtained. The reaction source terms are added for this computation, which corresponds to the cell startup process after being connected to work. Finally, computations of the dynamic process during step and sinusoidalchanges in operating conditions are conducted. The purpose of this computation is to know the transient response characteristics of fuel cell, and analyze dynamic performance of fuel cell.

All the coupled, non-linear model equations, including mass, momentum, species, temperature conservation equations, were converted to the finite-difference form by the control volume method. Stringent numerical tests are performed to ensure that the solution is independent of the grid size. As a result, the $82 \times 20 \times 104$ mesh can provide sufficient spatial resolution. The uniform grid is partitioned in direction y and z, but non-uniform in direction x. Fig. 1(c) shows the computation grid that was used for the bipolar plate. The solutions of the velocity com-

ponent equations are obtained in a staggered control volume. The coupled fluid velocity fields and pressure are solved by semi-implicit method for pressure-linked equations consistent (SIMPLEC) arithmetic. Then, the species and energy transport equations are computed after fluid velocities are obtained. Updating parameters based the computed results; the external iteration is conducted until the resolution is convergent. In this paper, the convergent criterion is that relative errors of all variables are less than 10^{-4}. In order to obtain the polarization curves, the method employed in this paper is to solve average current for a given voltage, which can guarantee solution stability and convergence. The time step for transient solution is 0.02 s.

This model is implemented into the commercial CFD code Fluent 6.1, with custom developed user-subroutines that consider the physicochemical processes associated with PEM fuel cells.

2.5. Physical properties

Mass diffusion coefficient of species i can be obtained through mass weight average of binary diffusion coefficient:

$$D_i = \sum_j m_i \cdot D_{i,j} \tag{17}$$

where the binary diffusion coefficient $D_{i,j}$ is defined as [17]:

$$pD_{i,j} = 3.64 \times 10^{-8} \left(\frac{T}{\sqrt{T_{c,i} \cdot T_{c,j}}} \right) \cdot (T_{c,i} \cdot T_{c,j})^{5/12} \cdot (p_{c,i} \cdot p_{c,j})^{1/3} \cdot \left(\frac{1}{M_i} + \frac{1}{M_j} \right)^{1/2} \tag{18}$$

And for the porous media as diffusion layer, the diffusion coefficient should be correlated by considering the effect of porosity and tortuosity factor. Furthermore, liquid saturation is considered to affect species diffusion coefficient. Thus, the effective mass diffusion coefficient can be determined as:

$$D_i^{\text{eff}} = \begin{cases} (1-s) \cdot D_i, & \text{channel} \\ (1-s) D_i \cdot \varepsilon^{1.5}, & \text{diffusion layer and catalyst layer} \end{cases} \tag{19}$$

The effective heat conductivity can be defined as [18]

$$\lambda_{\text{eff}} = \begin{cases} k_f, & \text{channel} \\ -2k_s + \left(\dfrac{\varepsilon}{2k_s + k_f} + \dfrac{1-\varepsilon}{3k_s} \right)^{-1}, & \text{porous media} \\ k_s, & \text{solid plate} \end{cases} \tag{20}$$

Local membrane conductivity σ_{mem} not only affects current density of the cell, but also determines temperature distribution inside the cell. Thus, it is important to obtain an accurate prediction of membrane conductivity, which is a function of water content and temperature of membrane. We adapt a widely used experiential equation summarized by Springer and Zawodinski [2]:

$$\sigma_e^{\text{ref}} = \begin{cases} 0.005139\lambda - 0.00326, & \lambda \geq 1 \\ \text{constant}, & \lambda < 1 \end{cases} \tag{21}$$

where σ_e^{ref} is the reference protonic conductivity under temperature 303 K and λ is the membrane water content. It can be correlated by considering temperature effect:

$$\sigma_e(T) = \sigma_e^{\text{ref}} \exp\left[1268 \left(\frac{1}{303} - \frac{1}{T} \right) \right] \tag{22}$$

The relation between water content λ at membrane surface and water vapor activity can be described by experiential equation as [19]:

$$\lambda = \begin{cases} 0.043 + 17.81a - 39.85a^2 + 36.0a^3, & 0 < a < 1 \\ 14 + 1.4(a-1), & 1 \leq a \leq 3 \\ 16.8, & a \geq 3 \\ 22, & \text{liquid water existence} \end{cases} \tag{23}$$

where a stands for water vapor activity at membrane surface. Water content is assumed to increase linearly from 14 under saturation to 16.8 under activity 3, because the experimental data for membrane content under activities 1–3 is scanty. Water vapor activity at membrane surface a can be defined as:

$$a = \frac{X_w p}{p^{\text{sat}}} \tag{24}$$

where p^{sat} is saturation vapor pressure corresponding to local temperature. The experiential expression equation between saturation vapor pressure and temperature is obtained by fitting

Table 1
Physics parameters and base conditions

Quantity	Value
Operating temperature (K)	353.15
Length of the channel (cm)	5.0
Channel width (cm)	0.1
Width of plate out channel (cm)	0.1
Channel thickness (cm)	0.1
Bipolar plate width (cm)	41 × 0.1
Diffusion layer thickness (cm)	0.025
Catalyst layer thickness (cm)	0.0028
Membrane thickness (cm)	0.005
Shoulder width (cm)	0.1
Operating voltage (V)	0.65
Pressure of anode inlet (kPa)	1 × 101.3
Pressure of cathode inlet (kPa)	1 × 101.3
Exchange current density of anode (A m^{-2})	100
Exchange current density of cathode (A m^{-2})	1000
Specific area of catalyst layer (m^{-1})	1.4×10^5
Velocity at the anode inlet (m s^{-1})	2.46
Velocity at the cathode inlet (m s^{-1})	13.15
Humidity of anode inlet stream (%)	80
Humidity of cathode inlet stream (%)	100
Condensation rate (s^{-1})	1.0

saturation vapor pressure under different temperature [3]:

$$\log_{10} p^{\text{sat}} = -2.1794 + 0.02953T - 9.1837 \times 10^{-5}T^2 + 1.4454 \times 10^{-7}T^3 \quad (25)$$

3. Results and discussion

Parameters of the fuel cell dimensions and the base operating case used in the computation of this study are listed in Table 1. Other physical parameters can be obtained from Bernardi and Verbrugge [1], or solved by method introduced in this literature.

3.1. Dynamic characteristics during startup process

The variations of hydrogen and oxygen concentration in the x–z plane at half height of channel with time during startup process are illustrated in Figs. 2 and 3. First of all, hydrogen concentration increases and oxygen concentration decreases along with flow for the electrochemical reaction. Although, both of them are consumed in the reaction, but there exist net water transporting from anode to cathode along with proton transfer, which cause the hydrogen concentration increase relatively because the molecular weight of water is much larger than hydrogen. Comparing these two pictures, we can also find that the time for hydrogen approaching steady-state value is longer, about

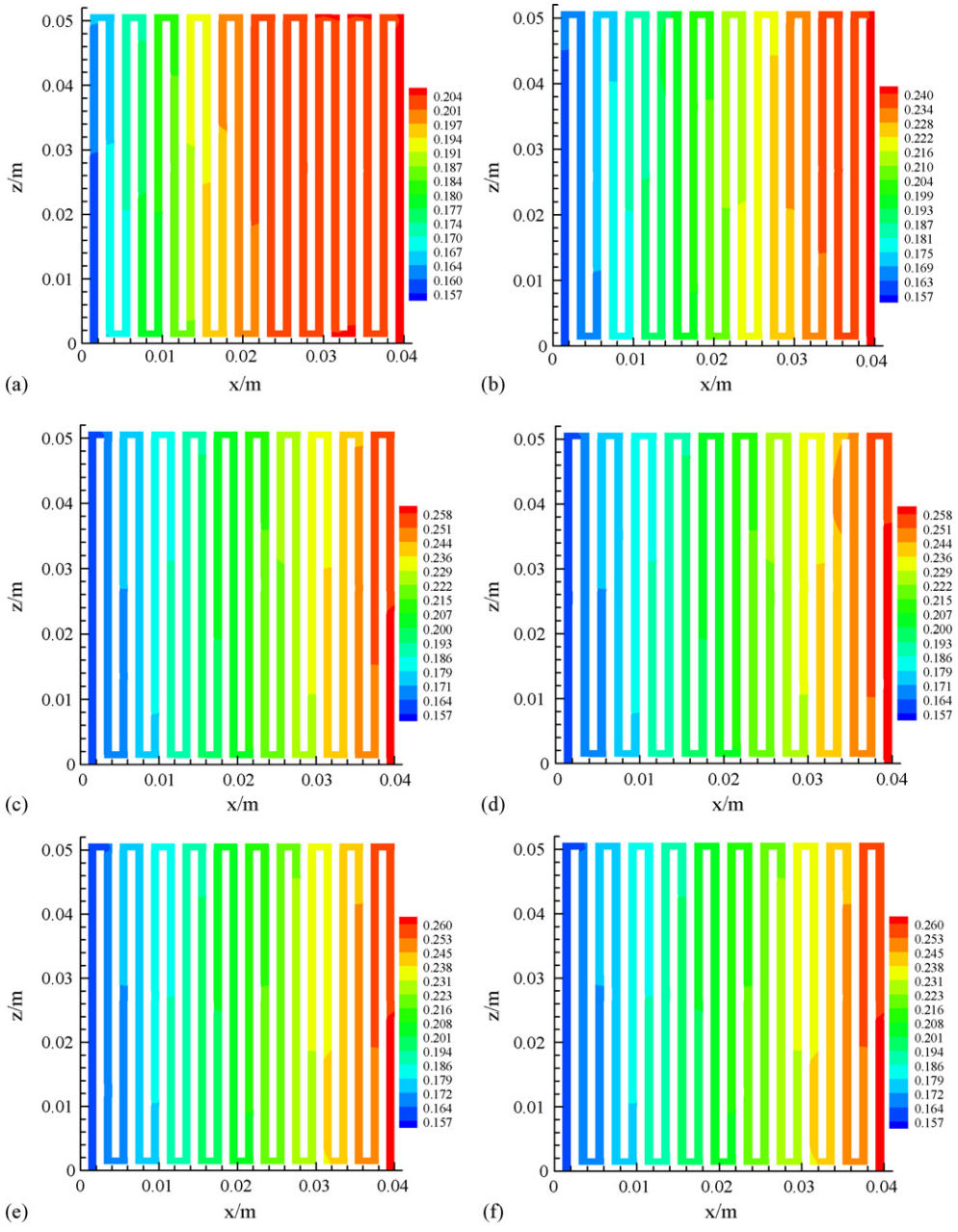

Fig. 2. Variations of hydrogen concentration in the x–z plane at half height of anode channel with time (a) $t = 0.3$ s, (b) $t = 0.6$ s, (c) $t = 0.9$ s, (d) $t = 1.2$ s, (e) $t = 1.5$ s and (f) $t = 1.8$ s.

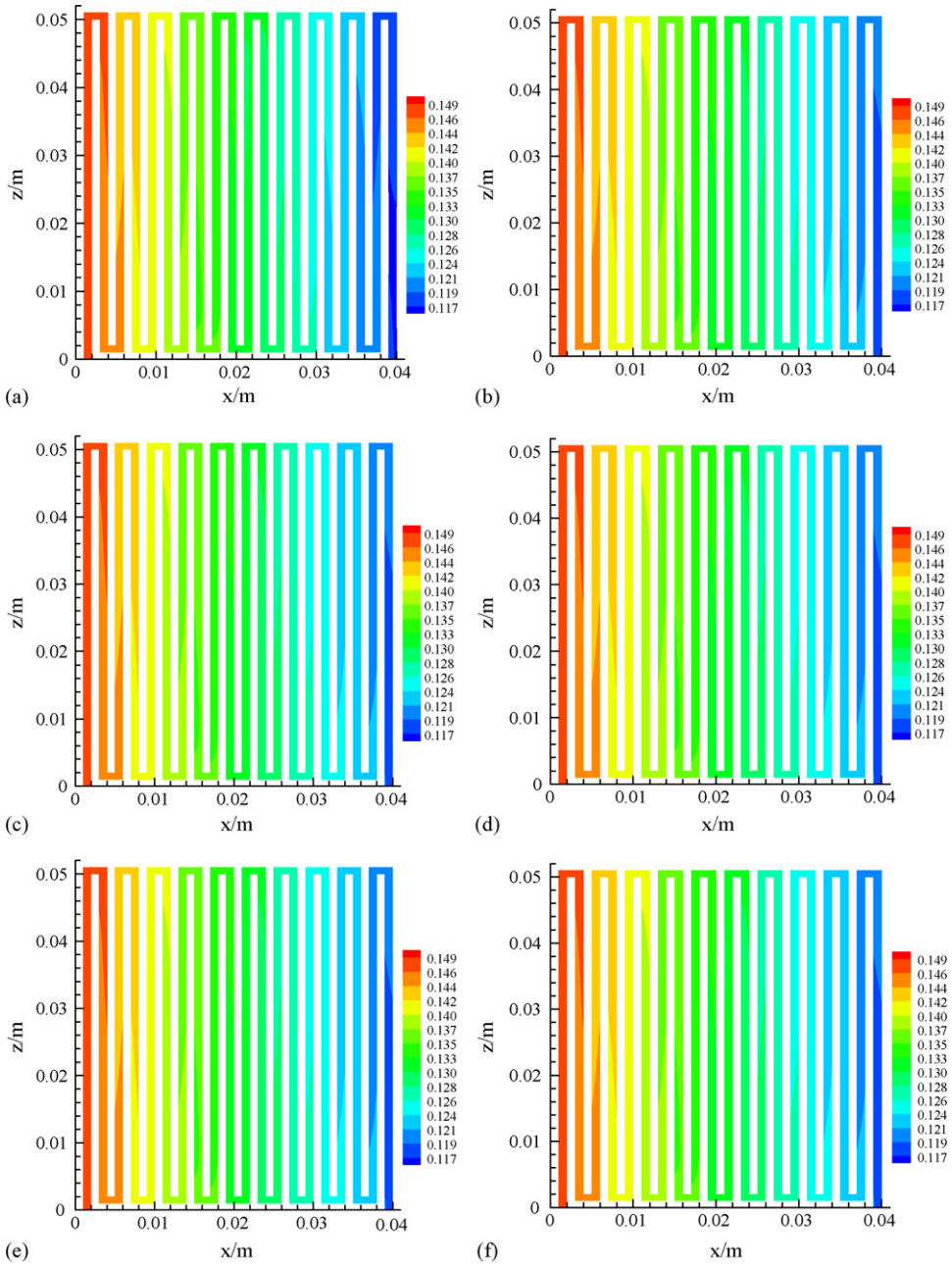

Fig. 3. Variations of oxygen concentration in the x–z plane at half height of cathode channel with time (a) $t = 0.3$ s, (b) $t = 0.6$ s, (c) $t = 0.9$ s, (d) $t = 1.2$ s, (e) $t = 1.5$ s and (f) $t = 1.8$ s.

1.2–1.5 s, in contrast, the time for oxygen approaching steady-state value is relatively shorter, about 0.6–0.9 s. The reason for this is mainly that the velocity in the cathode channel is faster than that in the anode channel, so the reactants can be provided by convection more quickly, i.e., the convection mass transfer takes up a major position, although the diffusion coefficient of hydrogen is larger than that of oxygen. We can also say that mass transfer is more important than the reaction rate because the oxygen reaction rate is much slower than the hydrogen reaction, i.e., the time constant of electrochemical reaction is very short in contrast to that of mass transfer.

Fig. 4 plots variations of the local current density with time during the startup process. Similarly, local current density decreases from the inlet to the outlet during the consumption of reactants. The time in approaching the steady-state value is also very short, about 0.6–0.9 s. This time is very close to the time required by oxygen concentration approaching steady state, which indicates that the time constant of the cell is determined by oxygen transfer. Because the current density is the main reflection of cell operation characteristics, it enough to imply that the startup time of the fuel cell is very short and of the order of second. Thus, a PEMFC can match the requirement as a power sources for transportation such as an electric vehicle. Actually, for a whole powering system, there exist many secondary systems each requiring some response time and the startup time of a PEMFC system is a second order effect; however, this is beyond

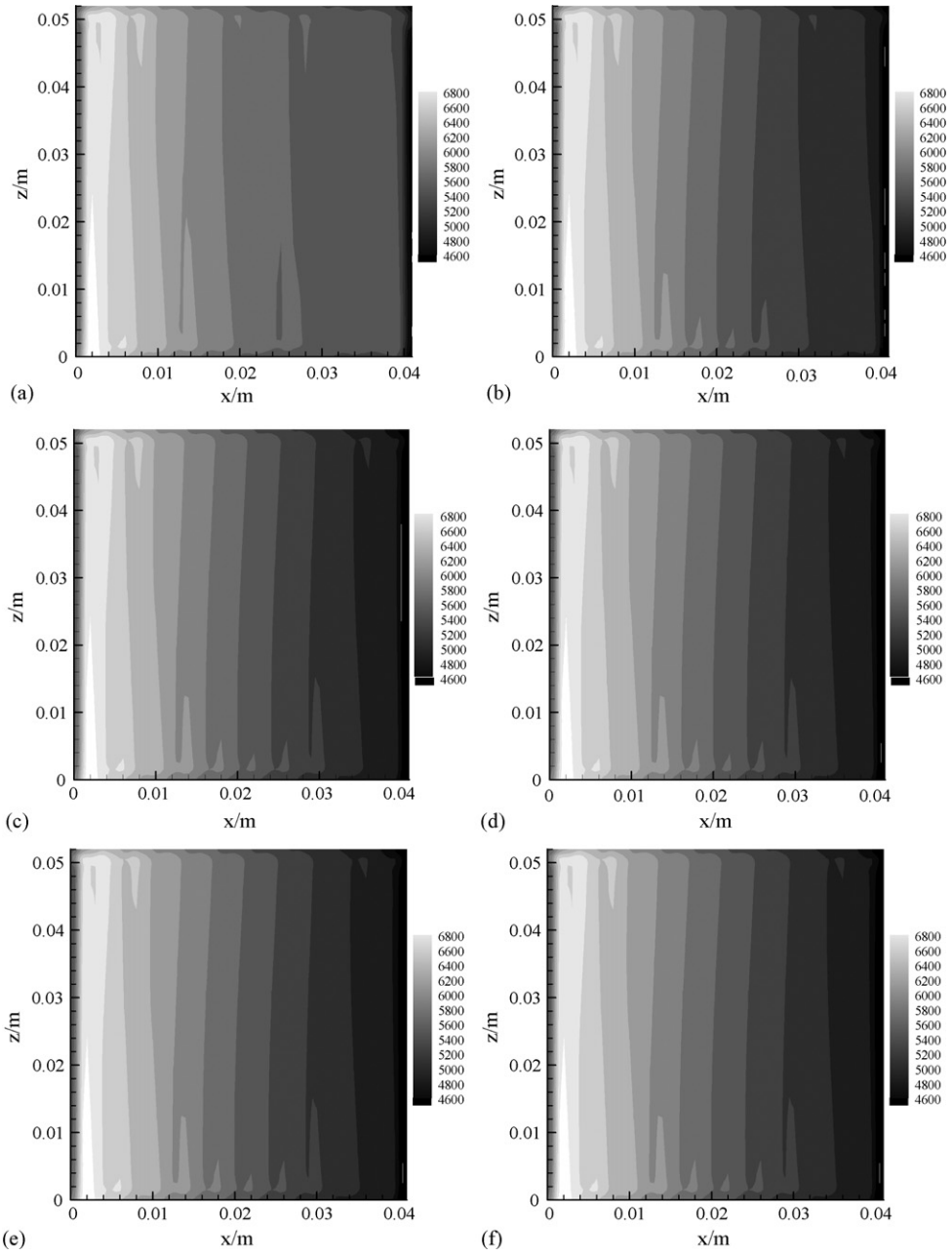

Fig. 4. Variations of local current density with time (a) $t = 0.3$ s and (b) $t = 0.6$ s, (c) $t = 0.9$ s, (d) $t = 1.2$ s, (e) $t = 1.5$ s and (f) $t = 1.8$ s.

the research range of this paper, but it is an important subject for our future research.

Fast startup under normal temperature is the prominent advantage of a PEMFC, which is different from other fuel cells. The computed variations of cell characteristics with time during the startup process are shown in Fig. 5: (a) pressure loss of the anode, (b) pressure loss of the cathode, (c) average temperature on the membrane surface of the cathode side, (d) oxygen concentration in the catalyst layer of the cathode, (e) hydrogen concentration in the catalyst layer of the anode and (f) average current density. Pressure loss for the anode is smaller than for the cathode; the main reason is that the inlet velocity of the cathode gas stream is higher than that of the anode. Furthermore, the pressure losses of both anode and cathode are smaller than without reaction. The average temperature on the membrane surface of the cathode side increases with time until a stable state is reached; this is because the reaction emits thermal energy. Similar to Fig. 2, the hydrogen mass fraction in the anode increases with time, this is because more water moves from the anode to the cathode during electrochemical reaction, then causes the mass fraction of hydrogen to increase relatively. The oxygen mass fraction decreases during consumption, which is similar to the decrease of local current density. Also, it can be found that there exists an interesting undershoot phenomenon for pressure loss of the anode and oxygen concentration of the cathode, but other variables have not shown this phenomenon. Altogether, the characteristic parameters reach a steady-state value in less than 2 s, i.e., the startup time of PEMFC is very short.

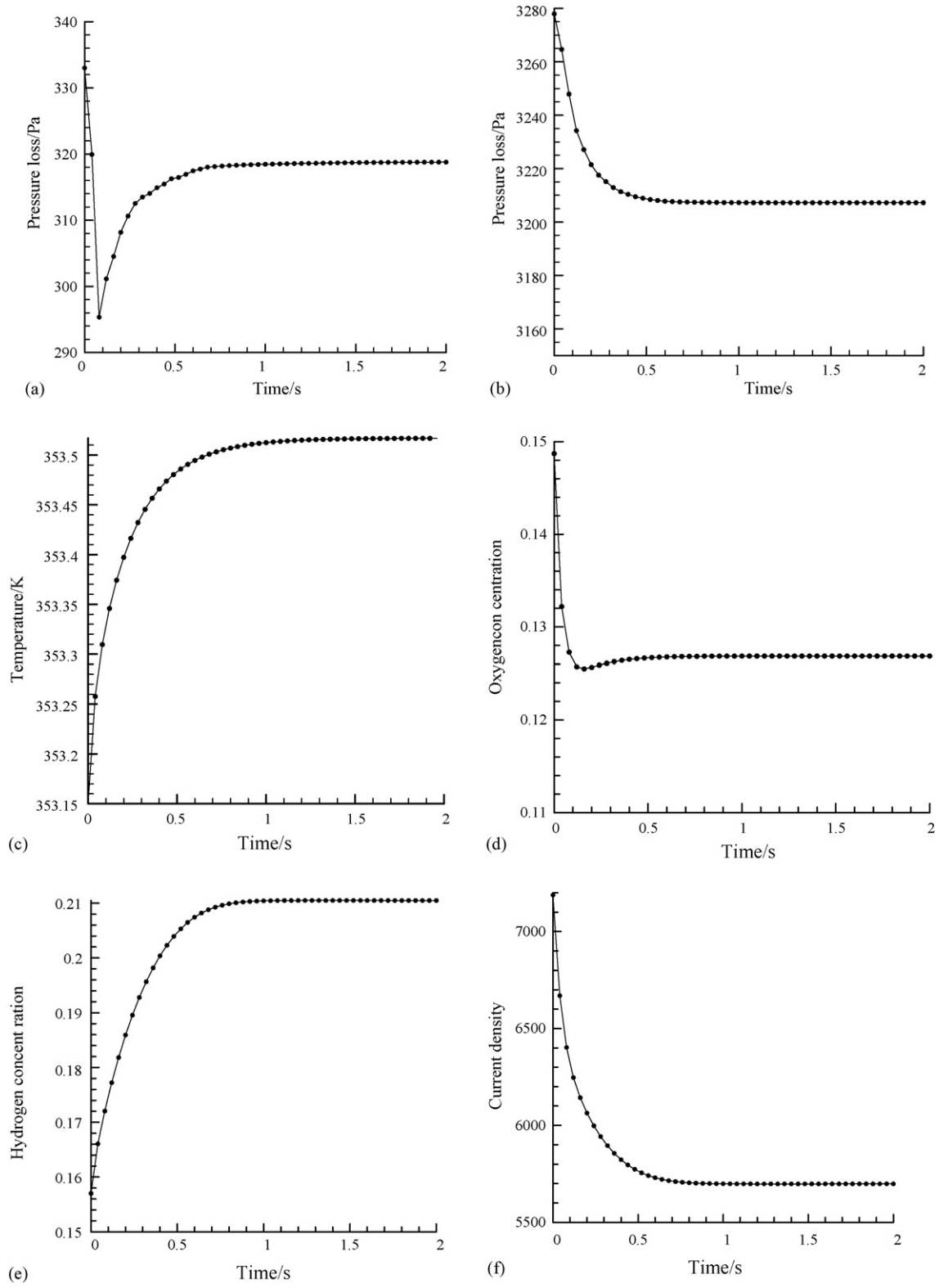

Fig. 5. Characteristic parameters variation during startup process. (a) Anode pressure loss, (b) cathode pressure loss, (c) average temperature on the membrane surface of the cathode side, (d) oxygen concentration in the catalyst layer of cathode side, (e) hydrogen concentration in the catlyst layer of anode side and (f) average current density ($A\,m^{-2}$).

3.2. Dynamic response during step change in operating cases

The following results were computed with a step change in one operating parameter, keeping the others constant. The temperature on the membrane surface of the cathode side was higher than in the other domains, so it was used as the research object in the following discussion.

Fig. 6 illustrates the dynamic response of the characteristic parameters during a step change in the stoichiometry flow ratio of the cathode inlet, which changes between 1.0 and 1.5 periodically. Fig. 6(a) shows a step change in the stoichiometry flow ratio, and Fig. 6(b and c) are the dynamic responses of the corresponding temperature of the membrane surface of the cathode side and the average current density of the fuel cell. It was found that the change in stoichiometry flow ratio had little effect on the temperature, about 0.02 K. The main reason is that the stoichiometry flow ratio increases, current density increases, and more heat was be produced; however, on the other hand more thermal energy can be removed by the higher velocity gas stream, serving as an effective refrigerant, and thus the total increase of temperature is very small. Increasing the inlet stoichiometry flow ratio can increase the cell performance effectively, i.e., the change of current density is larger, 5688–5768 A m^{-2}. The reason is that the reactants can be provided in time and the products can be removed faster. Response times of the cell to a step change between both stoichiometry flow ratios are very close, about 0.5 s. This indicates that the fuel cell can stabilize in a short time during a step change in the stoichiometric flow ratio. There exists a small overshoot of the average current density when the stoichiometry flow ratio changes from large to small, by contrast, an undershoot of the average current density occurs when the stoichiometry flow ratio changes from small to large. The temperature increases when the stoichiometric flow ratio increases, and vice versa, however, there does not exist any overshoot and undershoot phenomenon during the change process.

Fig. 7 shows the dynamic response behavior during a step change in the cathode inlet stream humidity, i.e., the relative humidity changes between 100 and 80% in the cycle. Fig. 7(a) plots the step change in the relative humidity, Fig. 7(b and c) show the corresponding dynamic responses of the temperature on the membrane surface of the cathode side and the average current density. It was found that the temperature changes about 0.1 K during the step change in the relative humidity, however the current density had relatively large change, from 5688 to 6400 A m^{-2}. When the humidity changes from large to small, the average current density increased and there existed a weak overshoot phenomenon. When the humidity changed from small to large, the average current density decreased and there existed an undershoot behavior. The temperature increased when humidity decreased, and vice versa, however, there did not exist any overshoot or undershoot phenomenon. The temperature will achieve a steady state in a shorter time than the current density during the step change in the cathode inlet stream humidity, of 0.7 and 1.4 s, respectively.

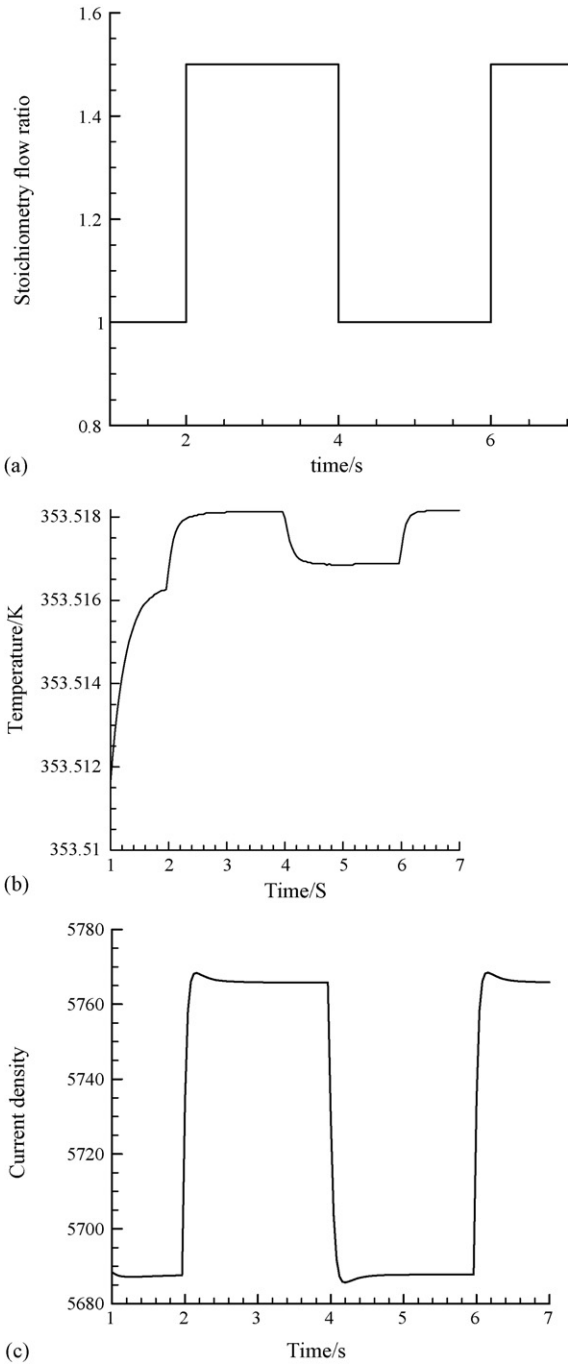

Fig. 6. Dynamic response of fuel cell during step change in stoichiometry flow ratio at cathode inlet. (a) Stiochiometry flow ratio at cathode inlet, (b) average temperature on the membrane surface of the cathode side and (c) average current density (A m^{-2}).

Fig. 8 shows the dynamic response during a step change in the operating voltage, which changes between 0.65 and 0.7 V in the cycle. Fig. 8(a) plots the step change in the operating voltage, and Fig. 8(b and c) illustrate the corresponding dynamic response of the temperature on the membrane surface of the cathode side and the average current density. It can be seen from the figures that the temperature has a small change of about 0.1 K during the step change in the operating voltage, however

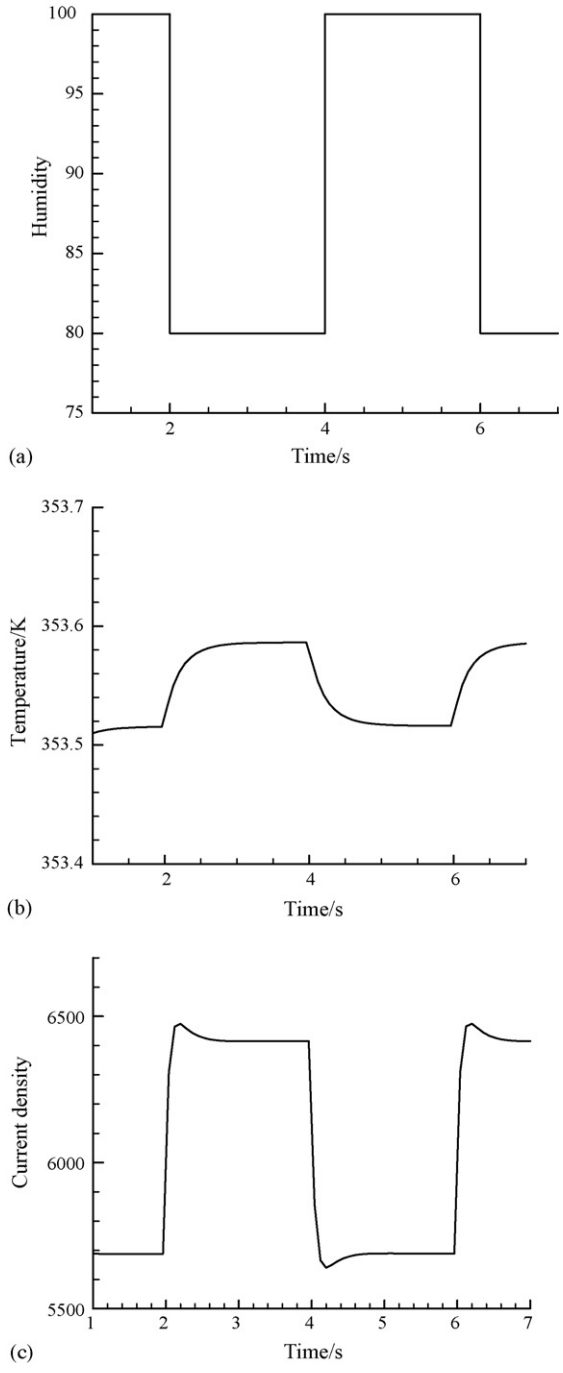

Fig. 7. Dynamic response of fuel cell during step change in cathode inlet stream humidity. (a) Cathode inlet stream humidity, (b) average temperature on the membrane surface of the cathode side and (c) average current density (A m^{-2}).

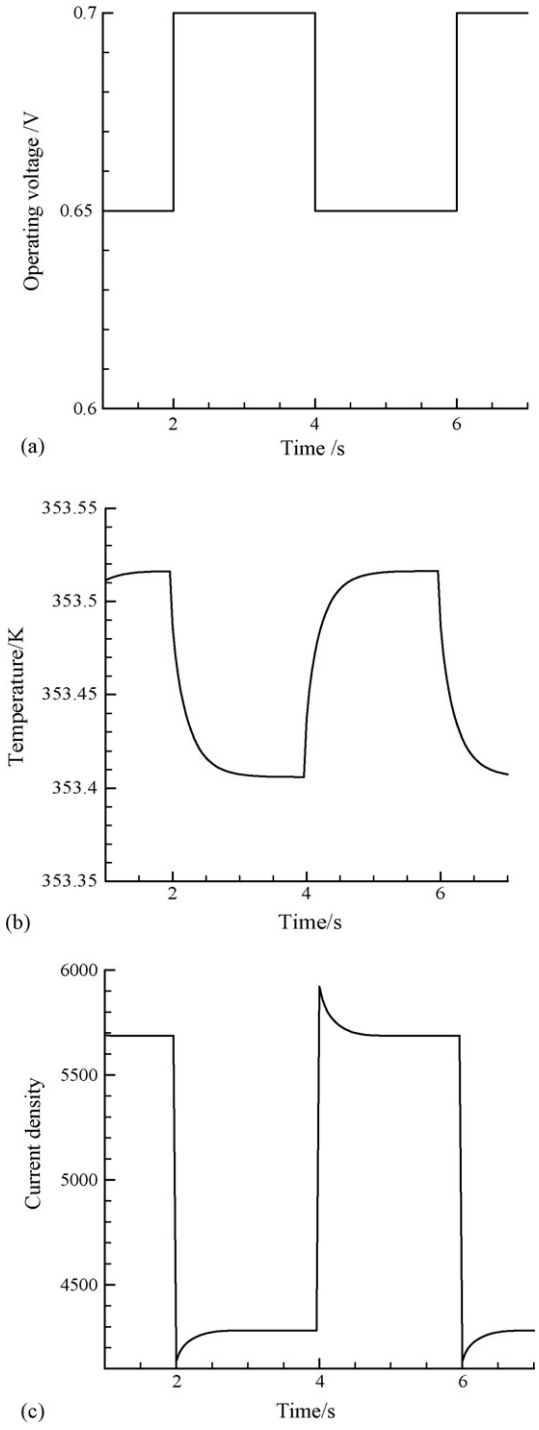

Fig. 8. Dynamic response of fuel cell during step change in operating voltage. (a) Operating voltage, (b) average temperature on the membrane surface of the cathode side and (c) average current density (A m^{-2}).

the current density change was relatively large, from 4300 to 5688 A m^{-2}. In the higher cell voltage case, the current density was lower and the temperature was lower for small ohmic heating effect. During a step change in cell voltage, there existed an obvious overshoot and undershoot phenomenon of current density, of about 200 A m^{-2}; however, the temperature did not show this phenomenon. The current density achieved a steady state in a shorter time, about 0.5 s, however the temperature achieved steady state in about 1.8 s.

3.3. Dynamic response behavior during sinusoidal change in operating cases

The following results are computed with a sinusoidal change in one characteristic parameter, keeping others constant. The purpose of this computation is to know the effect of a sinusoidal change on the cell performance.

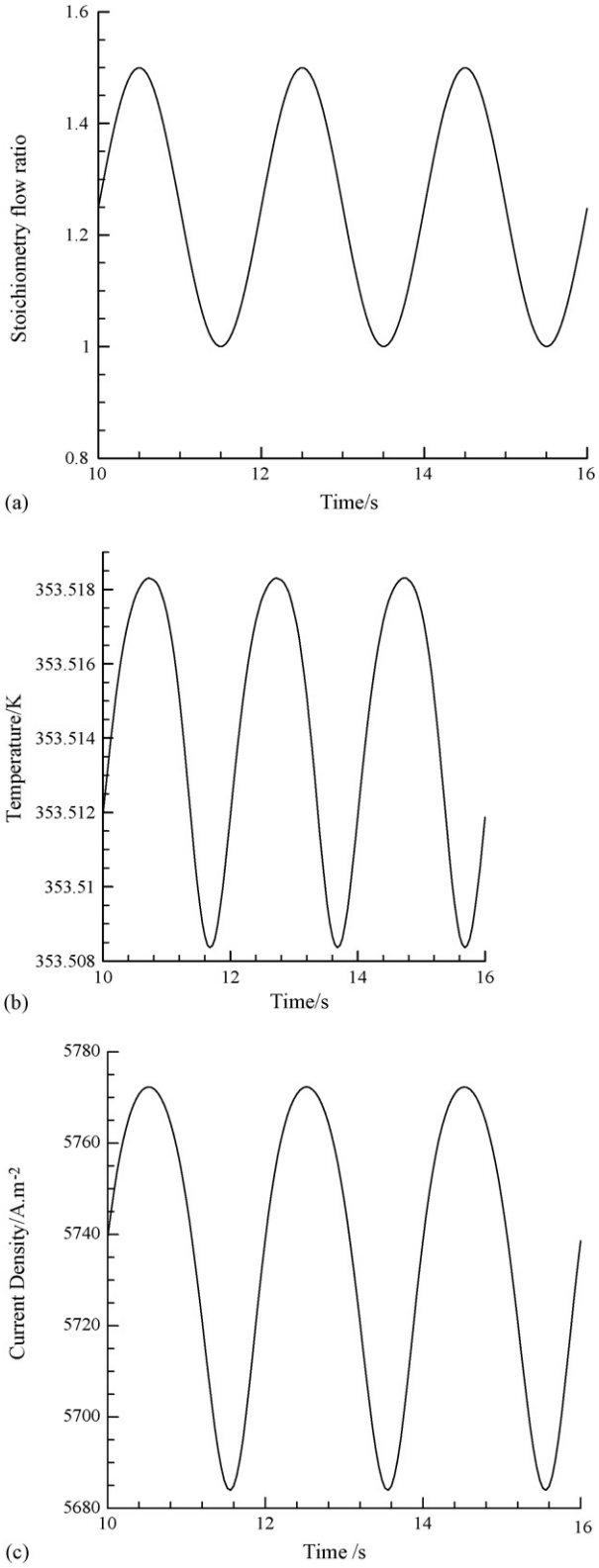

Fig. 9. Dynamic response of fuel cell during sinusoidal change in stoichiometry flow ratio at cathode inlet. (a) Stoichiometry flow ratio of cathode inlet, (b) average temperature on the membrane surface of the cathode side and (c) average current density.

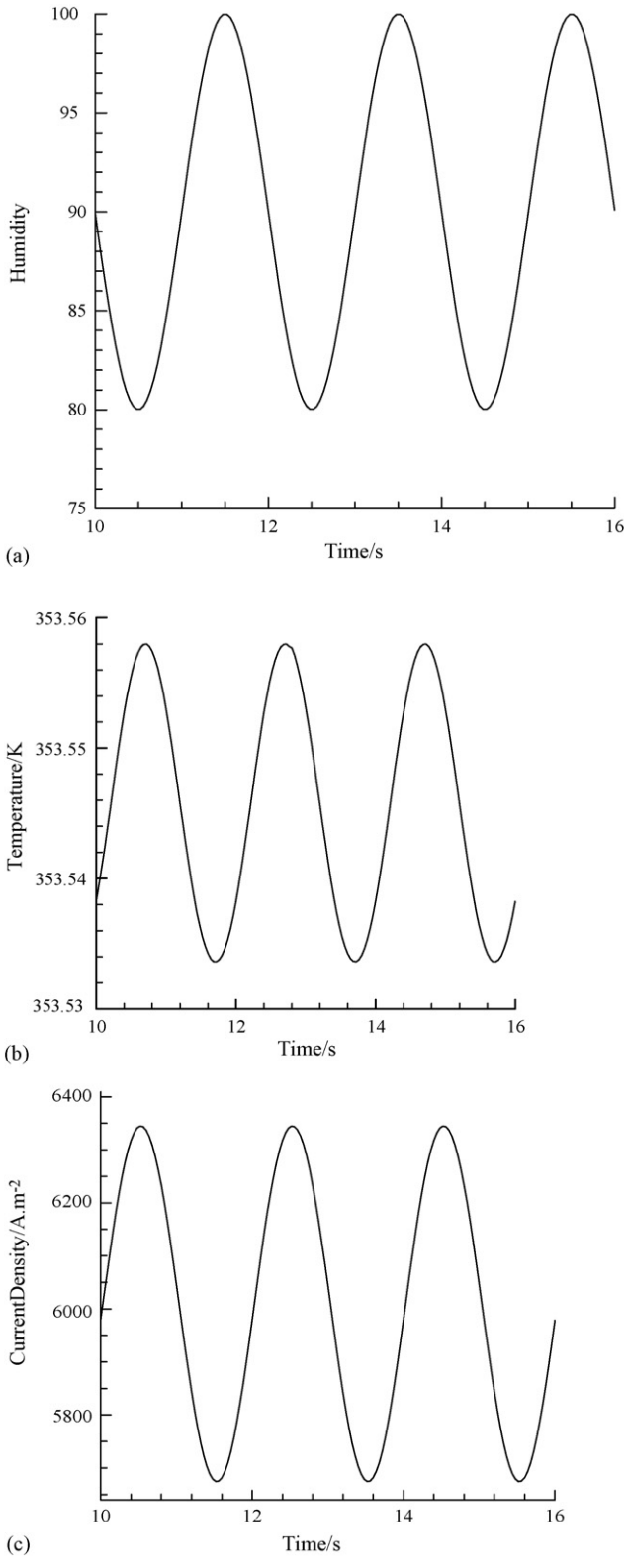

Fig. 10. Dynamic response of fuel cell during sinusoidal change in cathode inlet stream humidity. (a) cathode inlet stream humidity, (b) average temperature on the membrane surface of the cathode side and (c) average current density.

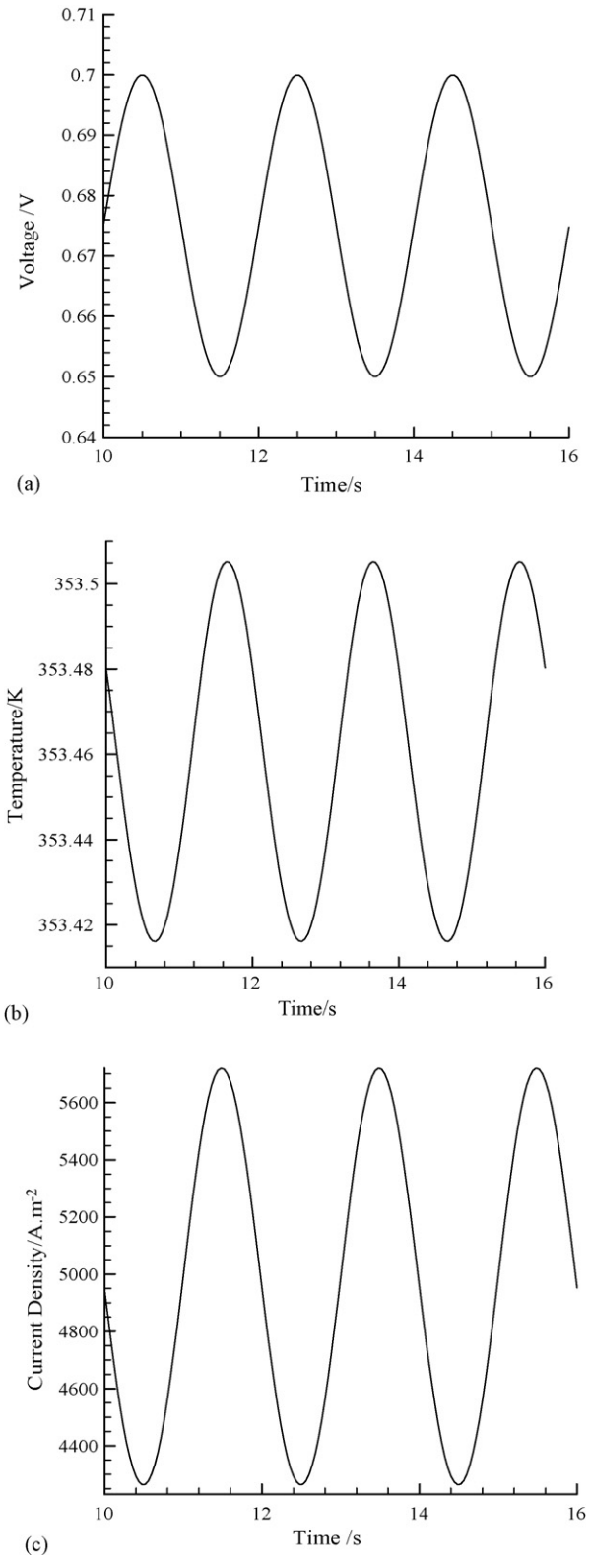

Fig. 11. Dynamic response of fuel cell during sinusoidal change in operating voltage. (a) Operating voltage, (b) average temperature on the membrane surface of the cathode side and (c) average current density.

Fig. 9 illustrates the dynamic response during a sinusoidalchange in the stoichiometry flow ratio of cathode inlet stream. Fig. 9(a) shows a sinusoidal change of the stoichiometry flow ratio of the cathode inlet stream, and Fig. 9(b and c) are the dynamic response behaviors of the corresponding temperature on the membrane surface of the cathode side and the average current density. It can be seen that the temperature and current density increase along with increase of the stoichiometry flow ratio, vice versa, decreases along with the decrease of the stoichiometry flow ratio. The process from high stoichiometry flow ratio to low stoichiometry flow ratio and from low stoichiometry flow ratio to high stoichiometry flow ratio is not very symmetrical; the change of value close to the upper limit is slower than that close to lower limit. Comparing to a step change, the upper limit and lower limit of temperature and current density are very close, but there does not exist any overshoot and undershoot phenomenon for the current density for the slow change of stoichiometry flow ratio.

Fig. 10 shows the dynamic response behavior during a sinusoidal change in the cathode inlet stream humidity, i.e., relative humidity changes from 100 to 80% in cycle. Fig. 10(a) plots the sinusoidal change of the relative humidity, Fig. 10(b and c) are the corresponding dynamic responses of the temperature on the membrane surface of the cathode side and the average current density. It was found that the temperature changed little, about 0.1 K, however the current density had a relatively large change, from 5688 to 6400 A m^{-2}. When the humidity changed from high to low, the average current density increased, and the temperature increased, and vice versa, the current density and temperature decreased. Comparing to a sinusoidal change in the stoichiometry flow ratio, the process from high humidity to low humidity and from low humidity to high humidity was almost symmetrical.

Fig. 11 shows dynamic response during sinusoidal change in cell voltage, between 0.65 and 0.7 V in the cycle. Fig. 11(a) plots the sinusoidal change in cell voltage, and Fig. 11(b and c) illustrate the corresponding dynamic response of the temperature on the membrane surface of the cathode side and the average current density. It was found that the temperature was little changed, less than 0.1 K, however the current density changed relatively much more, from 4300 to 5688 A m^{-2}. Under a higher cell voltage, the current density is lower and the temperature was lower for a small ohmic heating effect. This is a suitable polarization relationship between the current density and operation voltage.

4. Conclusions

A transient, three-dimensional and single-phase mathematical model was developed to investigate the dynamic response behavior of the characteristic PEMFC parameters such as temperature and current density during the startup process and step change and sinusoidal changes in stoichiometric flow ratio of the cathode inlet stream, the cathode inlet stream humidity and the cell voltage. Interesting undershoot/overshoot behavior of some of the variables was found. The computed results indicate that the dynamic response processes of PEMFCs are very fast, only

about 1–2 s, which is similar to most other reported simulation results, however this is significantly different from the time constant in Wang and Wang [11], the main reason is that the time change of liquid water in the membrane is considered in their paper. The results also show that this kind of low temperature fuel cell can be suitable for equipment requiring a quick startup power source such as an electrical vehicle.

Acknowledgements

The authors wish to express their thanks to Natural Science Foundation of Zhejiang Province of P.R. China (Grant No. Y106161).

References

[1] D.M. Bernardi, M.W. Verbrugge, A mathematical model of the solid-polymer-electrolyte fuel cell, J. Electrochem. Soc. 139 (1992) 2477–2491.
[2] T.E. Springer, T.A. Zawodinski, Polymer electrolyte fuel cell model, J. Electrochem. Soc. 138 (1991) 2334–2342.
[3] S. Dutta, S. Shimpalee, J.W. Van Zee, Three-dimensional numerical simulation of straight channel PEM fuel cells, J. Appl. Electrochem. 30 (2000) 135–146.
[4] G.L. Hu, J.R. Fan, S. Chen, Y.J. Liu, K.F. Cen, Three-dimensional numerical analysis of proton exchange membrane fuel cells (PEMFCs) with conventional and interdigitated flow fields, J. Power Sources 136 (1) (2004) 1–9.
[5] J.C. Amphlett, et al., A model predicting transient responses of proton exchange membrane fuel cells, J. Power Sources 61 (1996) 183.
[6] M. Wöhr, Bolwin, W. Schnurnberger, Dynamic modeling and simulation of a polymer membrane fuel cell including mass transport limitations, Int. J. Hydrogen Energy 23 (3) (1998) 213–218.
[7] H.P.L.H. Van Bussel, et al., Dynamic model of solid polymer fuel cell water management, J. Power Sources 71 (1998) 218–222.
[8] S. Um, C.Y. Wang, Computational fluid dynamics modeling of proton exchange membrane fuel cells, J. Electrochem. Soc. 147 (12) (2000) 4485–4493.
[9] S. Yerramalla, A. Davari, A. Faliachi, et al., Modeling and simulation of the dynamic behavior of a polymer electrolyte membrane fuel cell, J. Power Sources 124 (2003) 104–113.
[10] P.R. Pathapati, et al., A new dynamic model for predicting transient phenomena in a PEM fuel cell system, Renewable Energy 30 (2005) 1–22.
[11] Y. Wang, C.Y. Wang, Transient analysis of polymer electrolyte fuel cell, Electrochim. Acta 50 (2005) 1307–1315.
[12] S. Kim, S. Shimpalee, J.W. Van Zee, The effect of reservoirs and fuel dilution on the dynamic behavior of a PEMFC, J. Power Sources 137 (2004) 43–52.
[13] S. Kim, S. Shimpalee, J.W. Van Zee, The effect of stoichiometry on dynamic behavior of a proton exchange membrane fuel cell (PEMFC) during load change, J. Power Sources 135 (2004) 110–121.
[14] Y. Wang, C.Y. Wang, Dynamics of polymer electrolyte fuel cells undergoing load changes, Electrochim. Acta 51 (2006) 3924–3933.
[15] C.Y. Wang, Fundamental models for fuel cell engineering, Chem. Rev. 104 (2004) 4727–4766.
[16] Y. Wang, C.Y. Wang, Modeling polymer electrolyte fuel cells with large density and velocity changes, J. Electrochem. Soc. 152 (2005) A445–A453.
[17] R. Bird, et al., Transport Phenomena, Wiley, New York, 1960.
[18] V. Gurau, H. Liu, S. Kakac, Two-dimensional model for proton exchange membrane fuel cells, AICHE J. 44 (1998) 2410–2422.
[19] T.A. Zawodzioski, C. Derouin, S. Radzinski, et al., Water uptake by and transport through Nafion 117 mambrane, J. Electrochem. Soc. 140 (1993) 1041.